Vibration-Induced Wetting

Ofer Manor
James R. Friend
Leslie Y. Yeo
Micro/Nanophysics Research Laboratory, RMIT University, Melbourne, Victoria, Australia

Abstract
An overview of the influence of substrate vibration on the wetting of drops and films is presented. We initially consider the basic physics associated with the displacement of a three-phase contact line (CL), that in the context of liquids under vibrational excitation, lead to steady or periodic wetting and dewetting phenomena. To differentiate between the mechanisms that give rise to the various characteristic behavior observed, we delineate vibration-induced wetting and spreading dynamics into two broad categories, distinguished by the magnitude of the viscous penetration length (associated with the thickness of the viscous boundary layer flow) excited immediately above the vibrating substrate. Under relatively low-frequency excitation, the viscous penetration length is large, extending the effects associated with the viscous forcing in the boundary layer flow far beyond the submicron three-phase CL region, thus reducing the net viscous stress in the vicinity of the CL region. The variation in the three-phase contact angle and any CL displacement that arises is then mainly periodic, influenced by the dynamic shape oscillations of the liquid body induced by the vibration. In contrast, the viscous penetration length for high-frequency excitation is small, confined within a length scale commensurate with that of the CL region, hence rendering a viscous flow capable of varying the contact angle and inducing steady CL displacement, especially on substrates with high surface energies.

INTRODUCTION

Vibrational excitation of a finite liquid mass may render periodic or steady changes in the wetted area of a supporting solid substrate by altering the liquid–solid three-phase contact angle (CA) and displacing the corresponding three-phase contact line (CL). Such vibration-induced wetting of substrates may be intuitively categorized into two general types of excitation, namely, periodic and steady wetting.

Periodic wetting typically takes place under *low-frequency* vibration. The longitudinal pressure waves (i.e., sound waves) generated in the liquid due to the vibrating substrate have wavelengths that are usually large relative to the characteristic length of the liquid body at these low frequencies. To leading order, the pressure field in the liquid therefore does not vary spatially; as such, viscous effects associated with the propagation of sound waves are usually negligible, and a type of potential flow usually arises,[1,2] except perhaps in the vicinity of the solid substrate, where a thin viscous boundary layer exists.[3]

More specifically, the characteristic *low-frequency* range utilized to excite sessile drops in the literature is usually around 0.1–10 kHz, rendering the viscous penetration length within the range of tens of microns—large in comparison to the length scale associated with the submicron CL region. Consequently, this viscous flow has little influence on the CA itself. Such 0.1–10 kHz frequency vibration is instead known to produce shape oscillations of the free liquid boundary leading to oscillatory, although not generally harmonic, displacement of the CL. This results in repeated wetting and dewetting of the substrate once the substrate vibration intensity is sufficient to unpin the CL when CA variations exceed that bounded by the CA hysteresis range.[4,5] Similar periodic wetting and dewetting of substrates could also take place under the influence of spatially heterogeneous vibrations, such as transverse standing waves on the solid substrate. Depending on the spatial velocity variations along the solid substrate, second-order spatial pressure variations in the supported liquid mass could then arise, which are capable of displacing the liquid to a more energy-favorable position.

Steady wetting, on the other hand, is often excited by *high-frequency* vibration (typically 1 MHz–1 GHz) that results in a submicron viscous penetration length.[6,7] As such, most of the momentum associated with the viscous flow immediately adjacent to the solid is concentrated within a thin layer having a thickness comparable to the submicron characteristic length scale of the CL region. Consequently, the flow within this thin viscous layer is capable of bringing about a steady change in the CA beyond the hysteresis region.

We provide an overview of vibration-induced wetting in which we first focus on the mechanisms for CL displacement, an indispensable phenomenon necessary to comprehend dynamic wetting processes, even when there is no explicit reference to CL displacement in the following discussion on vibration and wetting. We briefly consider equilibrium CA physics and the effect of surface roughness and

Encyclopedia of Surface and Colloid Science DOI: 10.1081/E-ESCS-120047379

nonhomogeneous surface chemistry on the energetic state of the liquid body and on CA hysteresis. We then consider the non-continuum and continuum physical mechanisms believed to render CL displacement and the underlying difficulties associated with the latter by reviewing the corresponding mathematical models invoked to reconcile the use of continuum models to describe liquid spreading. Subsequently, we review various wetting and dewetting mechanisms under low-frequency vibration that induce periodic and transient CL displacement. Finally, we discuss steady wetting phenomena under high-frequency substrate vibration, in which we highlight various acoustic–capillary mechanisms and their contribution to wetting upon interaction with the free surface of a drop.

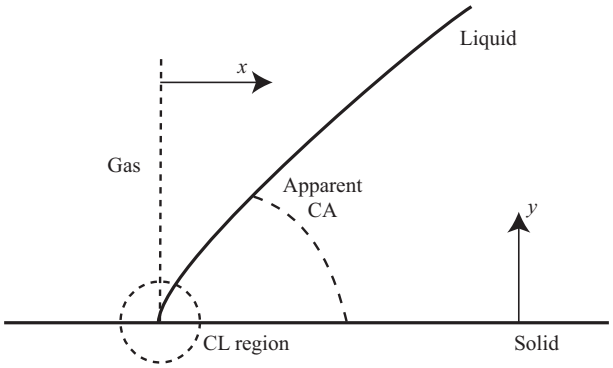

Fig. 1 Illustration of the apparent contact angle.

DYNAMIC WETTING

On an ideally smooth and chemically homogeneous solid substrate, a sessile liquid drop in equilibrium will possess a CA θ_Y defined by the Young equation as[3]

$$\cos\theta_Y = \frac{\gamma_{sg} - \gamma_{sl}}{\gamma}, \tag{1}$$

where γ_{sg}, γ_{sl} and γ are the solid–gas, solid–liquid and liquid–gas interfacial tensions, respectively. A further contribution to θ_Y arises due to tension imposed by the CL curvature, which results in an additional term in Eq. 1; this contribution is, however, small and can generally be neglected unless the CL possesses curvature of nanoscale order. Equation 1 is only satisfied when the drop is at equilibrium such that a finite CA appears between the liquid and the solid phases; fully wetting liquid–solid systems imply no such equilibrium and a better description for the condition at the CL is given by the wetting parameter

$$s = \gamma_{sg} - (\gamma_{sl} + \gamma), \tag{2}$$

representing the net tension that promotes wetting. The apparent CA θ_e (i.e., the measured CA) on an ideal solid surface is the same as θ_Y. Non-ideal solid surfaces or constrained liquid geometries, however, may cause θ_e to deviate from θ_Y in order to satisfy a global energy minimum.[8–11] In the process of dynamic wetting or dewetting, θ_Y is bounded by Eq. 1, maintaining a value which solely corresponds to the surface energy associated with the different phases, while the apparent CA in Fig. 1 may change during CL displacement.[3,12,13] Further, the apparent CL may become multivalued when approaching sharp corners (associated with substrate roughness) or experiencing chemical heterogeneity, giving rise to a local energy barrier for the CL displacement and requiring the CA to traverse different values as the CL is displaced on the substrate (Fig. 2), thus invoking CA hysteresis. The apparent CA on the substrate undergoing nano- or micro-scale heterogeneity

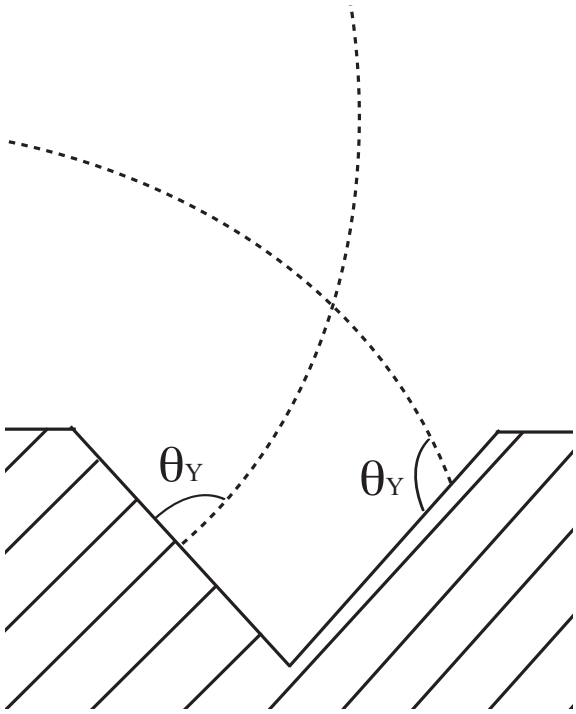

Fig. 2 Illustration of the multivalued apparent contact angle, shown by the dashed curve representing the liquid–gas interface as a result of surface roughness, represented here as a triangular dent, under the constraint of a single θ_Y.

posseses multiple values; the displacing CL is then subjected to additional stresses while crossing energy barriers imposed by the non-ideal solid surface that render deviations from the apparent CL at rest.

In Fig. 3, we sketch characteristic CA variations of the CL velocity, V_{CL}.[10,14–16] The CL is pinned while the CA is within the CA hysteresis range, bounded between the advancing CA θ_A and the receding CA θ_R. As the CA deviates from the hysteresis region, the CL is displaced at an increasing advancing or receding velocity; the velocity magnitude increasing with an increase in CA deviation from θ_A or θ_R. Further, under the influence of vibration,

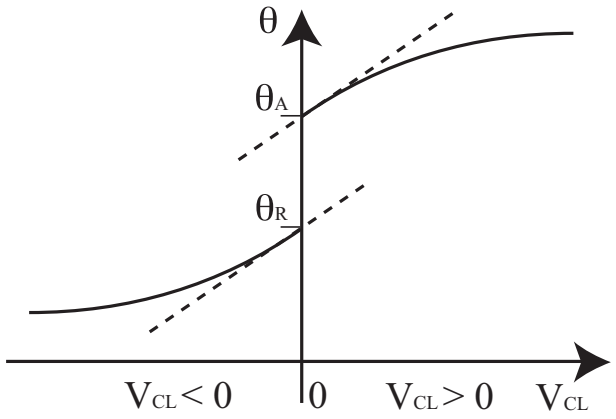

Fig. 3 Characteristic contact line (CL) velocity V_{CL} and variations in the contact angle (CA) θ, $0 < \theta < \pi$, where $\theta_A - \theta_R$ is the CA hysteresis region, rendering the CL pinned; the dashed lines are tangent to the CA curves at θ_A and θ_R.

the hysteresis region is known to decrease in magnitude; increasing the vibration intensity increases the vibrational energy transmitted to the drop, therefore allowing the CL to overcome a lower energy barrier, which would otherwise have resulted in the CL remaining locally pinned. CA hysteresis is therefore eliminated as θ_A and θ_R approach θ_Y beyond a certain vibration threshold, the hysteresis region may altogether vanish, allowing for a continuously displacing CL at all values of the CA.[17,18]

CL displacement incorporates contributions from both continuum and non-continuum mechanisms. The former consists of capillary contributions emerging from the different chemistries of the solid, liquid, and gas, secondary contributions emerging from the geometry of the advancing liquid front and mechanical contributions emerging from mass and momentum transport in the displacing and displaced gas or liquid that may be governed by viscous or convective flow regimes.[3,13,15,16,19–21] The latter primarily comprise contributions from molecular forces, such as electrical double layer or van der Waals forces, associated with the contact between the different solid, liquid, and gas phases involved. Using a continuum approach, Scriven[12] and Dussan & Davis[22] showed that the displacement of a simple CL between two fluids and a smooth solid plane imposes an infinite stress at the CL. An intuitive explanation of the source of this stress singularity at the displacing CL can be found in the no-slip condition, that is, a condition which implies that the velocity of two different phases, whether two fluids or a fluid and a solid, is equal everywhere at their mutual interface. In other words, the no-slip condition renders the CL velocity equal to the solid substrate velocity. Concurrently, imposing the constraint of a relative velocity between the liquid and the solid substrate at the CL therefore violates the no-slip condition, giving rise to an infinite stress. In reality, although the no-slip condition is generally appropriate, it breaks down in the vicinity of the CL where non-continuum processes take place to naturally relieve the otherwise unbounded stress. Different physical mechanisms were therefore suggested to model the behavior in the vicinity of the CL, the most common being a transient non-continuum diffusive adsorption of fluid molecules to the solid substrate, modeled as explicit or implicit slip lengths,[3,14,23–25] and the existence of an ultrathin precursor film that may be only tens of nanometers in thickness, materializing ahead of the visible CL[3,26] on fully wetting or partially wetting surfaces; ambient humidity may render the spontaneous presence of such thin water films on most surfaces.

Non-equilibrium transient diffusion of fluid, while adhering to the solid substrate, results in an effective slip near the CL. The slip behavior transforms back to the usual no-slip condition away from the CL, after the fluid molecules have had sufficient time to adhere to the solid. In terms of continuum theory, this process may be described with implicit or explicit Navier-type slip conditions. Formulating this condition, Dussan[27] and Huh & Mason[28] introduced a direct constraint on the relative velocity between a steady air–water interface and a solid plate immersed in the liquid at velocity V_{CL}. This condition artificially eliminates the stress at the CL by removing the solid immersion velocity at the CL while applying the no-slip condition far from it, that is,

$$\left.\begin{aligned} \mathbf{u}\cdot\mathbf{t} &= 0, \qquad y = 0, x \to 0, \\ \mathbf{u}\cdot\mathbf{t} &= V_{CL}, \qquad y = 0, x \to \infty, \end{aligned}\right\} \tag{3}$$

where $\mathbf{t}$ is the unit vector tangential to the solid surface, $\mathbf{u}$ the velocity vector, and the coordinates x and y are as illustrated in Fig. 1. Different continuous expressions bounding a complete slip condition at the CL to no-slip far away from the CL region were tested to examine the sensitivity of the full-slip to no-slip transition on the flow field. It was found that while the microscopic flow in the CL region was remarkably sensitive to the transition functionality, this was not true for the macroscopic flow outside the CL region. An additional condition suggested is a characteristic Navier slip length in the CL region in the form

$$(\mathbf{T}\cdot\mathbf{n})\cdot\mathbf{t} = \lambda V_{CL}, \qquad y = 0, x \to 0, \tag{4}$$

where $\mathbf{n}$ is the unit vector normal to the solid surface and $\mathbf{T}$ is the stress tensor. The slip length in which non-continuum effects take place in the CL vicinity is then $2\mu/\lambda$ in which μ is the shear viscosity and λ is an empirical coefficient. In a different study, Mason[29] used the adhesion time t_A required by the liquid molecules to physically adhere to the solid upon contact, during which time the no-slip condition is violated in order to justify the slip region in the CL vicinity and hence eliminate the drag forces:

$$\left.\begin{aligned} \mathbf{t}\cdot\left(\mathbf{T}\cdot\mathbf{n}\right) &= 0, \qquad y = 0, V_{CL}t_A > x > 0, \\ \mathbf{u} &= V_{CL}\mathbf{t}, \qquad y = 0, x > V_{CL}t_A. \end{aligned}\right\} \tag{5}$$

A different approach, employing an implicit slip condition, was suggested by Hocking[4,5] for small deviations in the CA from its hysteresis value where the velocity of the CL is under the constraint

$$\left.\begin{aligned} V_{\mathrm{CL}} &= C(\theta-\theta_{\mathrm{A}}), && \theta>\theta_{\mathrm{A}},\\ V_{\mathrm{CL}} &= 0, && \theta_{\mathrm{R}}<\theta<\theta_{\mathrm{A}},\\ V_{\mathrm{CL}} &= C(\theta-\theta_{\mathrm{R}}), && \theta<\theta_{\mathrm{R}}. \end{aligned}\right\} \tag{6}$$

This is graphically illustrated in Fig. 3 as dashed lines, representing linearization of the CA against V_{CL} curves just outside the CA hysteresis range; C is the empirical slope of the curves at θ_{A} and θ_{R}.

Fully wetted, that is, very hydrophilic, solids do not require the invocation of slip to justify CL displacement; either the solid is already covered by a finite thickness film or an ultrathin front-running liquid precursor film is formed,[30–32] relieving the stress in the vicinity of the CL. Either film mediates between the capillary and viscous forces acting in the macroscopic bulk of the CL and the capillary and long range molecular forces due to electrical double layer or van der Waals forces in the microscopic region of the CL. The microscopic CL region then effectively slides atop a thin layer of liquid adsorbed onto the solid, naturally relieving unbounded stresses. A capillary and viscous balance in the CL region spreading atop the fully wetted solid yields the Hoffman–Tanner rule[33–36]

$$\mathrm{Ca} \equiv \frac{\mu V_{\mathrm{CL}}}{\gamma} \propto \theta^3, \tag{7}$$

where $\mathrm{Ca} \equiv \mu V_{\mathrm{CL}}/\gamma$ is the Capillary number. On hydrophilic solid substrates, which allow for small apparent equilibrium CAs with the liquid θ_e, the spreading velocity of the CL follows a similar rule[3]

$$\mathrm{Ca} \propto \theta(\theta_e^2-\theta^2). \tag{8}$$

Further, matching between the macroscopic and microscopic parts of the CL[37,38] gives a closed form solution for small CAs associated with the spreading CL in the form[39]

$$\tan^3\theta = \tan^3\theta_e - 9\mathrm{Ca}\log\frac{A/6\pi\gamma}{L}, \tag{9}$$

where A is the Hamaker coefficient that defines a negative disjoining pressure between the substrate and free surface and L is the characteristic length of the liquid body. In fact, the universally weak logarithmic dependence of the asymptotic slope of the advancing wetting front $\tan\theta$ suggests that the dynamic CA is insensitive to the mechanism used to alleviate the CL stress singularity, whether it be the slip model in Eq. 4, the precursor film model discussed earlier, or the molecular force model expressed by the disjoining pressure in Eq. 9, at least for partially to fully wetting solids.[39,40]

On the other hand, when the spreading CA is large, CL displacement during the spreading of a viscous liquid may lead to a rolling mechanism wherein a recirculatory flow in the vicinity of the advancing CL transports liquid from the vicinity of the gas–liquid interface to the vicinity of the solid–liquid interface (or vice versa during dewetting). Further, when the CL velocity is large, that is, in large Ca systems, a nose forms above and ahead of the displacing CL during spreading to balance viscous and capillary stresses.[41] Nevertheless, these processes do not exclude the requirement for slip at the CL or a precursor film ahead of it to avoid unbounded stress.[22,42]

PERIODIC WETTING UNDER LOW-FREQUENCY VIBRATION

As briefly discussed in the "Introduction," low-frequency vibration of solid substrates that support a liquid body, such as sessile drops atop piston-like vibrators, can be viewed from the perspective that the wavelengths of the pressure wave (i.e., sound wave) they generate in the liquid are large compared to the characteristic length scale of the liquid body. To first approximation, therefore, the pressure field in the liquid is spatially isotropic and only varies in time with the oscillation of the solid phase. In these circumstances, viscous streaming in the bulk of the liquid outside a thin viscous boundary layer adjacent to the solid substrate may be ignored.[7] The influence of the viscous boundary layer on bulk flow and on CL dynamics may usually be ignored as well, since the boundary layer thickness (i.e., the viscous penetration length) is usually measured in tens and hundreds of microns, far beyond the submicron length scale of the CL vicinity and usually far below the length scale of the liquid bulk. The free surface then deforms in a periodic manner in response to periodic changes in the liquid internal transient pressure, mediated by the potential flow. This interfacial response eventually stabilizes around the natural drop frequency ω_n. For a spherical drop undergoing small shape deformations, this satisfies[43]

$$\omega_n^2 = \frac{n(n-1)(n+1)(n+2)}{(n+1)\rho}\frac{\gamma}{R^3}, \tag{10}$$

where n, ρ, and R are the natural frequency mode, liquid density, and drop radius, respectively. Equation 10 was subsequently extended to allow for a hemispherical drop atop a solid support.[1] Further, the interfacial response of a liquid body subject to planar thickness-mode vibration takes the form of Faraday waves[44,45] at one-half the excitation frequency, at least in the limit of shallow surface waves.

In addition, shape oscillations of an excited liquid body may render the liquid CL pinned or unpinned

subject to the vibration intensity being below or above an intensity threshold, which allow CA variations to exceed the CA hysteresis range. CA values above the hysteresis range yield stick-slip CL dynamics, in which the CL is displaced or pinned when the transient CA value is outside or inside the hysteresis range, respectively. The CL displaces outward from the liquid when the drop shape oscillations render $\theta > \theta_A$ and toward the liquid when the drop shape oscillations render $\theta < \theta_R$, as shown in Fig. 3. Further, the stick-slip CL dynamics reduces the natural frequency modes of the liquid body, shown for a puddle by Noblin et al.[47,48] and calculated for a drop by Lyubimov et al.[49] and Fayzrakhmanova & Straube[50] who used boundary conditions similar to Eq. 6 to describe the relationship between the drop's CA value and CL velocity.

A secondary effect of the substrate vibration is to alter the steady pressure field in the supported liquid that may induce drop displacement or steady patterning of free liquid surfaces. The relationship between pressure p and density ρ in an adiabatic system is given by[53,54]

$$p - p_0 = c_f^2 \left(\rho - \rho_0\right) + \frac{1}{2}\left(\frac{\partial c_f^2}{\partial \rho}\right)_0 \left(\rho - \rho_0\right)^2 + \ldots, \qquad (11)$$

where the subscript 0 refers to equilibrium values and c_f is the speed of sound in the liquid. Under harmonic vibrational excitation, the leading excess harmonic pressure on the left-hand side of Eq. 11 is proportional to the first term on the right-hand side and vanishes over long times. The second-order correction to the excess pressure, specified by the second term on the right-hand side of Eq. 11, however, retains a steady non-vanishing component, which to leading order is proportional to the magnitude of the Reynolds stress in the fluid ρU^2;[55] U is the substrate vertical displacement velocity amplitude. The excess steady pressure in the liquid then varies with the vibration (surface wave) wavelength, approaching a maximum at antinodal points and vanishing at nodal points. As seen in Fig. 4, this drives the displacement of drops toward antinodal points as well as the patterning of liquid films,[46,56,57] provoked by an interplay between the steady pressure gradient in the liquid and capillary force.

In another study, drops atop tilted substrates and under sufficient transverse vibration intensity were observed to climb *upward* against gravity.[51,58] The upward force on the drops was attributed to a combination of the asymmetrical vibration in the plane normal to the solid substrate due to its inclination with respect to the vertical vibration and the nonlinear frictional force between the drop and the substrate embedded in the CA hysteresis. This yielded a ratchet-like displacement mechanism that allows the drop to climb upward, slide downward, or maintain a similar position (Fig. 5). Another form of ratchet-like drop displacement, invoked directly by substrate vibration in this particular case, was observed under asymmetrical substrate longitudinal vibrations (i.e., substrate displacements tangent to the surface); the asymmetry is inherent in the vibration itself that comprises a faster displacement velocity in a certain direction, complemented by a lengthier period of retreat to impose no net displacement of the substrate.[52] The asymmetric inertial force ratchets the drop in the direction of force excess, allowing the drop CA to overcome the hysteresis region only in a particular direction. The excited drops are found to attain maximum velocities on hydrophobic substrates when the forcing frequency coincides with their resonance modes; the drops may however move in the opposite direction upon deviation of the excitation toward the nonresonance modes (Fig. 6).

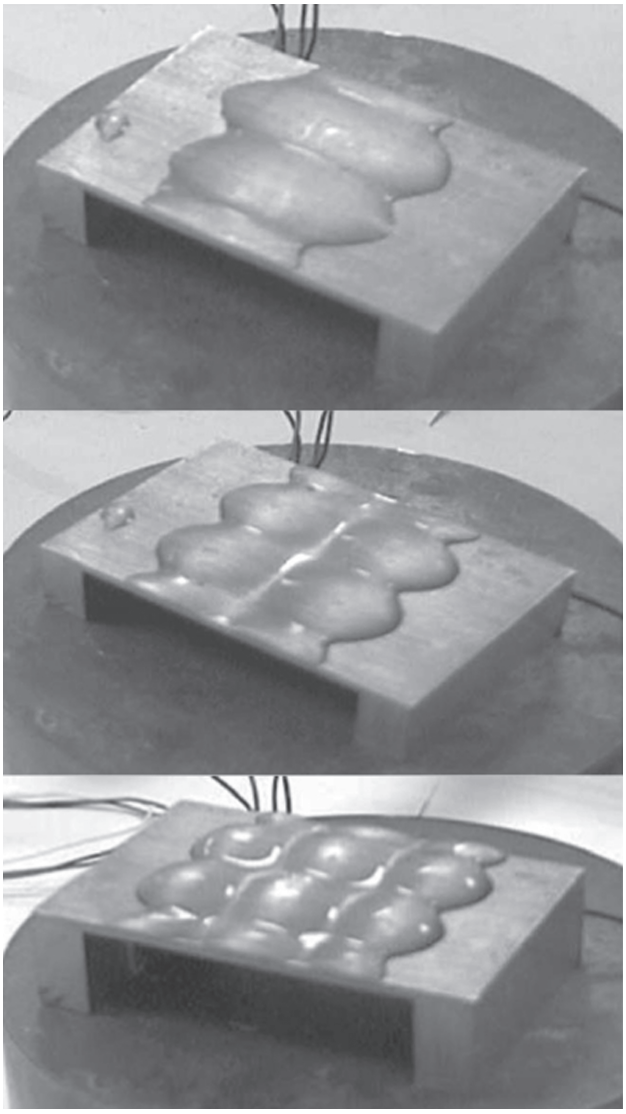

Fig. 4 Images showing the arrangement of a water film atop a rectangular membrane, vibrating at 30 kHz with different Lamb-wave resonance modes, in which ridges and valleys appear at vibration amplitude antinodes and nodes, respectively.
Source: From Scortesse, et al.[46]

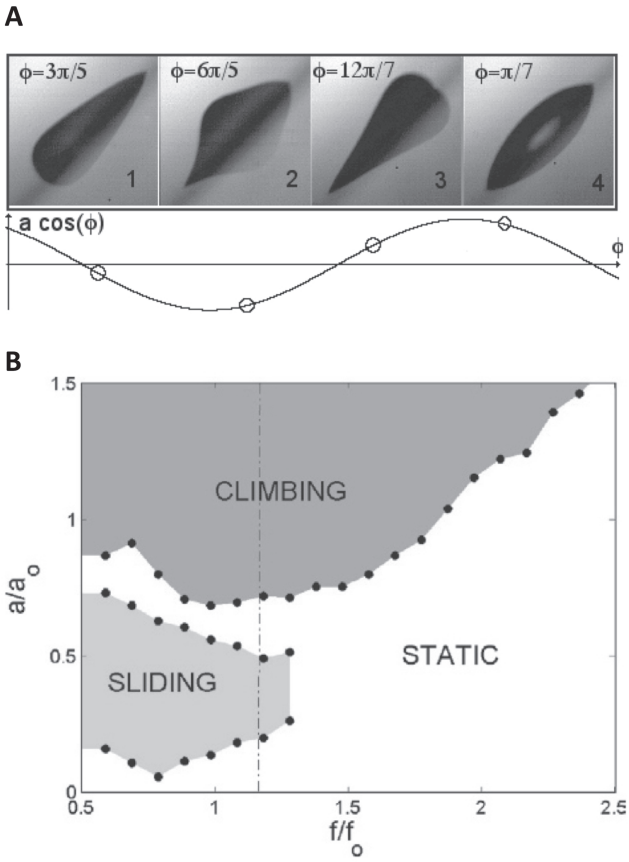

Fig. 5 (**A**) Side view images of a 5 µl drop with a kinematic viscosity of 31 mm^2/s placed on a plate that is inclined at $\alpha = 45°$ and vibrating at 60 Hz; the images show both the drop and its symmetric mirror reflection on the tilted plate. The corresponding phase of the plate acceleration, taken to be maximum at the phase origin, is shown below. (**B**) Phase diagram of the observed drop behavior; f_o is the drop resonance frequency; a and a_o are the substrate acceleration and acceleration at f_o, respectively.
Source: From Brunet, et al.[51]

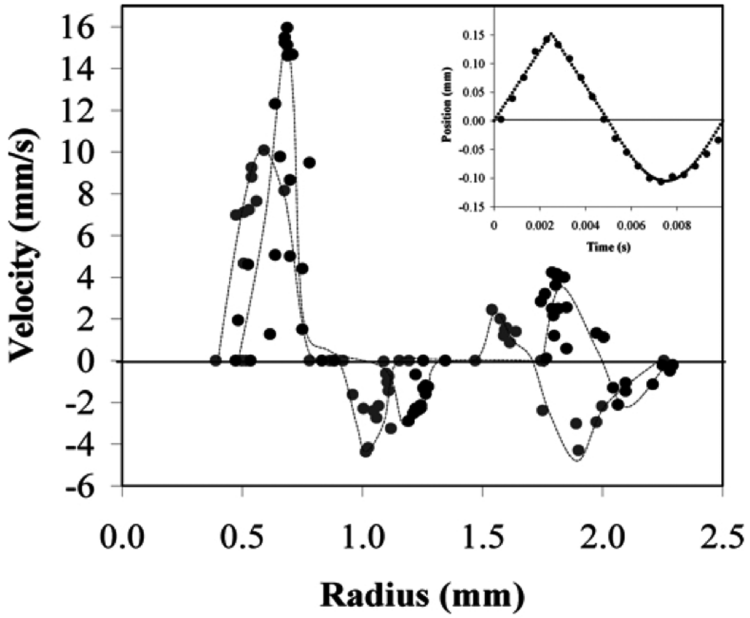

Fig. 6 Net advancing drop velocity as a function of the drop radius. The black and gray circles correspond to 100 and 120 Hz frequency excitation, respectively, with a longitudinal (along the surface) substrate wave displacement amplitude of 0.11 mm; the inset shows the asymmetric waveform indicating the longitudinal displacement of the substrate in each vibration cycle.
Source: From Daniel, et al.[52]

STEADY WETTING UNDER HIGH-FREQUENCY VIBRATION

In contrast to its low-frequency counterpart, high-frequency vibration is capable of producing viscous boundary layer flow whose momentum is concentrated within a submicron layer, capable of inflicting sufficient power at the vicinity of the CL to alter the CA between a liquid and the solid substrate such that its quasisteady value lies beyond the CA hysteresis region. Further, under high-frequency vibration, the wavelength of the sound wave emitted into the liquid is usually small with respect to the liquid body (with the exception of thin films), rendering attenuation of sound waves in the liquid and the appearance of several nonlinear phenomena that are typically suppressed in low-frequency vibration systems. These consist of the acoustic radiation pressure,[59,60] the net directional stress arising when sound waves impinge on the interface between phases of mismatched acoustic impedance, ρc_f, and Eckart streaming,[7,61,62] a long-range vortical flow generated due to the viscous attenuation of sound waves.

High-frequency vibration has been employed to drive microfluidics using very efficient piezoelectric actuators designed for transverse or lateral vibrations, or more complicated forms of surface vibrations encompassing Rayleigh and Sezawa surface acoustic waves (SAWs) as well as bulk acoustic waves (BAWs) including Lamb, surface-skimming bulk waves (SSBWs) and flexural waves in which *both* wave components along and transverse to the solid surface are present.[6,54] We will illustrate in the discussion to follow an example of curious high-frequency vibration induced wetting phenomena that have recently been discovered, where the excitation of a water drop by a simple 2 MHz transverse vibration results in wetting or dewetting, depending on the initial wettability of the substrate.

Manor et al.[63] investigated a case of a 2 µl sessile drop of deionized water excited by piston-like transverse substrate vibrations on a surface-coated lead zirconate titanate (PZT) thickness-polarized disk with frequency $f \approx 2$ MHz. The sound wavelength $\lambda_f = c_f/f \approx 0.75$ mm is then smaller than the 1 mm characteristic height of the drop. As such, the density and pressure fields inside the drop vary both in space and time and we can expect acoustic streaming and acoustic radiation pressure to influence the drop in response to the excitation. Figure 7A shows the response of the sessile drop when the substrate was coated with a thin film of PTFE (polytetrafluoroethylene), a highly hydrophobic substrate comprising an equilibrium CA $\theta_e \approx 120°$. At low-excitation velocity U, the CL remained pinned while the air–water interface was found to elongate vertically in the same direction as the incident sound wave emitted by the vibrating substrate due to transfer of wave momentum to the drop interface, i.e., the acoustic radiation pressure. Above an excitation velocity threshold, the CL was observed to unpin and the average value of the CA, fluctuating under the vibrational excitation (the CL dynamics follows the physics illustrated in Fig. 3). The average CA value was found to slightly decrease while remaining hydrophobic throughout the excitation velocity range employed; overall, the wetted area under the drop was observed to shrink due to drop elongation. The drop response when the substrate was coated with a thin polydimethylsiloxane layer, treated with toluene to increase the hydrophobicity such that the equilibrium CA is slightly below the hydrophobic limit $\theta_e \approx 88°$ (although the toluene treatment resulted in mild surface roughness), however, was found to be characteristically different, as illustrated in Fig. 7B. At low-excitation power when the CL remained pinned, the drop was observed to elongate vertically. However, when the excitation power was sufficient to unpin the CL, the drop was observed to spread over the solid substrate.

The discrepancy between the response of the water drops atop the different substrates highlight the different competing mechanisms that govern the geometry of the

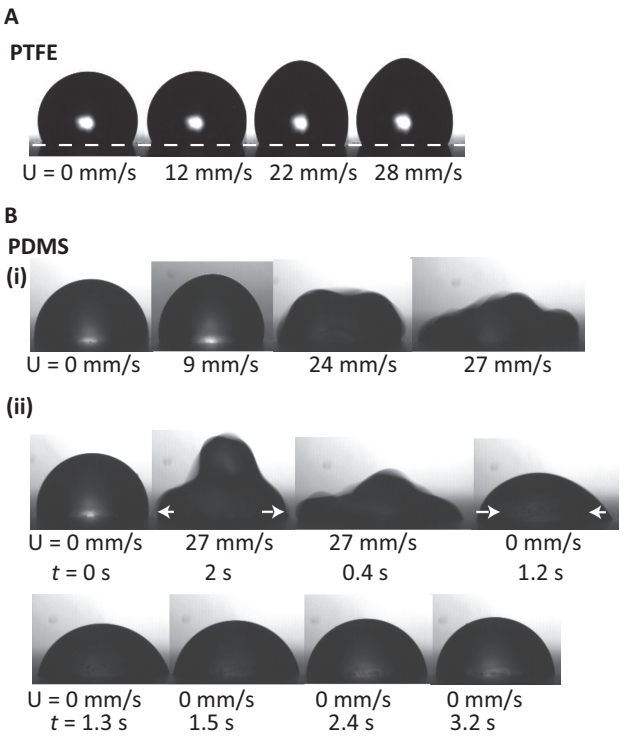

Fig. 7 Response of a 2 µl drop atop a PZT disk coated with (**A**) PTFE or (**B**-i) polydimethylsiloxane (PDMS) under varying substrate transverse velocity amplitudes U. The initially pinned CL unpins above $U = 12$ mm/s for PTFE and above $U = 9$ mm/s for PDMS; unpinned drops form quasisteady shapes on PTFE, whereas their counterparts on PDMS were observed to fluctuate rapidly, captured in the corresponding images for velocity amplitudes of 24 and 27 mm/s. (**B**-ii) Time series plot of the drop atop PDMS showing the initially spreading drop CL ($0 < t < 0.4$ s) which subsequently receded to its initial position as the power is relaxed ($t > 1.2$s); the arrows show the CL displacement direction. After spreading to its new quasisteady position, the excited CL continues to vibrate but without any net displacement at long times.
Source: From Manor, et al.[63]

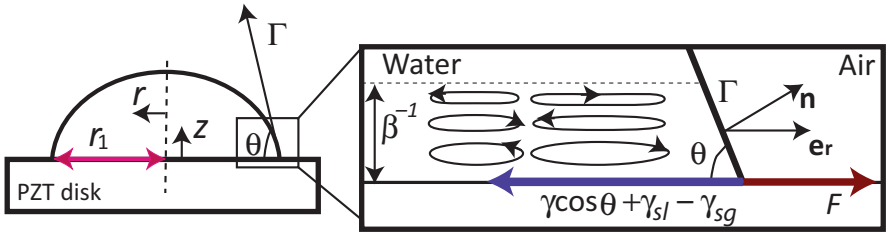

Fig. 8 Schematic of a drop atop a PZT ceramic disk with its axisymmetric axis illustrated as a dashed line; the inset to the right magnifies the CL region, where boundary layer flow of a characteristic thickness β^{-1} interacts with the air–water interface at Γ and contributes an integral acoustic tension F to the capillary force balance at the CL.
Source: From Manor, et al.[63]

excited drops. One mechanism is acoustic radiation pressure that impinges upon the free surface of the drop, thereby causing the drop to elongate upwards. The other mechanism is a viscous boundary layer flow, characteristically similar to the Schlichting boundary layer flow, whose extension near the drop edges interacts with the free surface of the drop in the CL vicinity, thus invoking an additional tension that acts to displace the CL outward such that the drop spreads on the substrate. Here, we focus on the latter mechanism responsible for the reversible CL displacement to a new equilibrium position under vibrational excitation. Incorporating the acoustic tension inflicted upon the CL into the quasistatic equilibrium force balance, as illustrated in Fig. 8,

$$\gamma \cos\theta + \gamma_{sl} - \gamma_{sv} = F, \tag{12}$$

then leads to a variation in the equilibrium CA θ from its initial value θ_0 in a manner similar to that in static electrowetting.[64] The interfacial stress, imposed by the viscous boundary layer flow **u**, is localized within a small region of thickness $\beta^{-1} \equiv \left(2\mu/\rho\omega\right)^{1/2} \simeq 0.4\ \mu$m near the solid such that the viscous flow is concentrated near the CL vicinity.[40,65,66] Here, $\omega = 2\pi f$ is the vibration angular frequency. The approximate radial Reynolds stress acting on the air–water interface Γ in the CL vicinity then gives the steady radial force per unit length along the CL:

$$F \approx \frac{\rho}{32\beta^{-1}}\left(Ur_1\right)^2 \cos^2\theta, \tag{13}$$

where U is the substrate vibration amplitude and r_1 is the radial length of the circular substrate–water interface. Substituting this in Eq. 12 then gives

$$\cos\theta - \cos\theta_Y = \mathrm{We}\frac{r_1}{\beta^{-1}}\frac{\cos^2\theta}{32}, \tag{14}$$

where $\mathrm{We} \equiv \rho U^2 r_1/\gamma$ is a Weber number associated with the mechanical power emitted into the liquid by the solid vibration through an area wetted by the base of the drop.

Simple qualitative analysis of Eq. 14 reveals that it satisfies the singular solution $\theta = 90°$, implying that an initial $\theta_Y = 90°$ will not be affected by the acoustic force at the CL, resulting in $\theta = 90°$. Further, this singular solution renders any initial $\theta_Y > 90°$ to remain hydrophobic while decreasing in magnitude ($\theta_Y > \theta > 90°$) under vibrational excitation, and any initial $\theta_Y < 90°$ to become more hydrophilic ($\theta_Y < \theta < 90°$) with vibration. While the experimental result in Fig. 7 shows limited spreading on mildly rough polydimethylsiloxane surfaces, a quantitative study of Eq. 14 suggests that a hysteresis-free ideal solid undergoing $\theta_Y < 90°$ may result in $\theta \to 0$ under moderate *We* values. Further, Eq. 13 reveals that the smaller the viscous penetration length β^{-1}, the larger the force inflicted upon the CL region. That is, the higher the excitation frequency and the lower the viscosity of the liquid, the more pronounced the influence of the viscous flow on the CA. Other studies on acoustic–capillary mechanisms, employing silicon oil as the liquid medium and higher-frequency vibrations together with different types of solid vibration modes, have observed similar sensitivities of the wetting process to the initial CA value and to the magnitude of the viscous penetration length.[67,68]

CONCLUSIONS

A brief overview of the influence of substrate vibration on the wetting of drops is presented. We first considered the non-continuum and continuum physical mechanisms believed to account for CL displacement and the underlying difficulties associated with the latter, as well as the corresponding mathematical models invoked to reconcile the use of continuum models to describe liquid spreading that subsequently govern wetting and dewetting mechanisms. We then considered liquids under vibration excitation that give rise to various wetting mechanisms, namely, steady and periodic displacement of the liquid–solid CL.

For the purpose of this overview, we classify vibration-induced wetting and spreading dynamics into two broad categories, characterized by the magnitude of the viscous penetration length. Low-frequency excitation renders a viscous penetration length large with respect to the length scale associated with the CL vicinity, where capillary and molecular forces determine CA and CL static and dynamic behavior. In these cases, periodic CL displacement, excited

by shape oscillations of the vibrated liquid body, arises. Specifically, such low-frequency vibration tends to excite capillary waves, such as Faraday waves at one-half the excitation frequency or harmonic oscillation of free liquid bodies at their natural frequency. The free surface excitation, whether capillary waves or natural frequency modes, render oscillatory change in the CA value that under sufficient excitation intensity overcomes the CA hysteresis, leading to periodic CL displacement and subsequently to a reduction in the frequency of the natural oscillation mode. Further, low-frequency–induced ratchet-like displacement of drops are observed to take place under the broken symmetry of vibrational excitation. In addition, imposing vibrational excitation neither transverse nor tangent to an inclined solid surface, drops are observed to climb upward against the action of gravity. The upward force is found to result from a combination of the mismatch between the vibration direction and the intrinsic direction of the solid surface (i.e., longitudinal or transverse with respect to the inclination of the solid surface) and the nonlinear friction embedded in the relationship between the CA value and the CL displacement. Similar mechanisms of ratchet-like drop displacement was observed and even used for the design of drop microfluidic platforms. In the case examined here, the ratchet-like mechanism is invoked by asymmetrical longitudinal vibrations that occur at an inclination with the solid surface. A faster displacement velocity in one direction, complemented by a lengthier period of retreat to impose no net displacement of the substrate, causes the drop to overcome CA hysteresis in only one direction, resulting in directional drop displacement. Another mechanism for wetting is related to secondary pressure effects in liquid bodies that are excited by spatially heterogenous vibrational amplitudes. These pressure gradients are found to yield transient wetting of liquid films or drops that spread or displace, respectively.

In contrast, high-frequency excitation endows the liquid with a viscous penetration length of similar magnitude to the length scale associated with the CL vicinity, practically "concentrating" the force associated with the viscous boundary layer flow in the CL vicinity to a level which may be sufficient to induce CL displacement, especially on high-energy surfaces; often, the liquid spreading is superimposed upon secondary periodic CL displacement due to spurious low-frequency vibrations of the liquid invoked by the high-power transmission associated with high-frequency vibration. Very different wetting phenomena are therefore observed with high-frequency vibration. For example, the liquid spreading dynamics under high-frequency vibration was observed to be dependent on the initial wettability state of the liquid on the substrate. A large initial CA is observed to prohibit liquid spreading under high-frequency vibration, whereas a small initial CA is observed to allow for liquid spreading over the substrate.

The displacement amplitude of the imposed vibrational excitation can also play a role in the wetting, either directly or indirectly. Periodic wetting, in which the CL is displaced primarily due to shape oscillations of a liquid body, is driven by dynamic pressure oscillations in the liquid. These pressure oscillations are proportional to the velocity amplitude of the vibrating surface, that is, the angular frequency multiplied by the displacement amplitude of the solid substrate. Steady wetting, on the other hand, while depending on the mechanical power associated with the vibration (which is proportional to the surface velocity of the substrate, squared), occurs when the viscous penetration length is of the same order of magnitude as the length scale associated with the capillary mechanisms that govern the CA. In this case, the viscous penetration length itself is determined in part by the vibration frequency and is independent of the vibration displacement amplitude. An increase in the substrate vibration velocity or displacement amplitude may thus influence the intensity of periodic or steady wetting but, at least to leading order, does not traverse the wetting dynamics across the two wetting mechanisms.

It is worth noting as a concluding remark that little remains understood about vibration-induced spreading, particularly that associated with high frequencies in which an abundance of rich phenomena has recently been uncovered.[67] The underlying mechanisms governing the spreading dynamics remains elusive, primarily due to the challenges associated with the mathematical difficulties encountered in analyzing the vast length and time scale separation, as well as the intricate nonlinear effects inherent in high-frequency excitation not evident in its low-frequency counterpart. Nevertheless, recent discoveries in this field have led to exciting new possibilities, particularly for driving fast and efficient microfluidic transport, and we remain confident that future advances will lead to a greater understanding of the physics underpinning this phenomenon.

REFERENCES

1. Strani, M.; Sabetta, F. Free vibrations of a drop in partial contact with a solid support. J. Fluid Mech. **1984**, *141*, 233–247.
2. Wilkes, E.D.; Basaran, O.A. Nonlinear oscillations of pendant drops. Phys. Fluids **1997**, *9*, 1512–1528.
3. de Gennes, P.G. Wetting: Statics and dynamics. Rev. Mod. Phys. **1985**, *57*, 827–863.
4. Hocking, L.M. Waves produced by a vertically oscillating plate. J. Fluid Mech. **1987**, *179*, 267–281.
5. Hocking, L.M. The damping of capillary–gravity waves at a rigid boundary. J. Fluid Mech. **1987**, *179*, 253–266.
6. Friend, J.R.; Yeo, L.Y. Microscale acoustofluidics: Microfluidics driven via acoustics and ultrasonics. Rev. Mod. Phys. **2011**, *83*, 647–704.
7. Lighthill, J. Acoustic streaming. J. Sound Vib. **1978**, *61*, 391–418.
8. Marmur, A. A guide to the equilibrium contact angles maze. In *Contact Angle, Wettability Adhesion*, Mittal, K., Ed.; Koninklijke Brill NV, Leiden, 2009; Vol. 6, 3–18.

9. Marmur, A. Contact angles in constrained wetting. Langmuir **1996**, *12*, 5704–5708.
10. Dussan, E.B.; Chow, R.T.P. On the ability of drops or bubbles to stick to non-horizontal surfaces of solids. J. Fluid-Mech. **1983**, *137*, 1–29.
11. Wolansky, G.; Marmur, A. The actual contact angle on a heterogeneous rough surface in three dimensions. Langmuir **1998**, *14*, 5292–5297.
12. Scriven, L. Hydrodynamic model of steady movement of a solid/liquid/fluid contact line. J. Colloid Interface Sci. **1971**, *35*, 85–101.
13. Cox, R.G. The spreading of a liquid on a rough solid surface. J. Fluid Mech. **1983**, *131*, 1–26.
14. Dussan, E.B. On the spreading of liquids on solid surfaces: Static and dynamic contact lines. Annu. Rev. Fluid Mech. **1979**, *11*, 371–400.
15. Blake, T.D.; Haynes, J.M. Kinetics of liquid/liquid displacement. J. Colloid Interface Sci. **1969**, *30*, 421–423.
16. Blake, T.D.; Shikhmurzaev, Y.D. Dynamic wetting by liquids of different viscosity. J. Colloid Interface Sci. **2002**, *253*, 196–202.
17. Andrieu, C.; Sykes, C.; Brochard, F. Average spreading parameter on heterogeneous surfaces. Langmuir **1994**, *10*, 2077–2080.
18. Decker, E.L.; Garoff, S. Using vibrational noise to probe energy barriers producing contact angle hysteresis. Langmuir **1996**, *12*, 2100–2110.
19. Marmur, A. Equilibrium and spreading of liquids on solid surfaces. Adv. Colloid Interface Sci. **1983**, *19*, 75–102.
20. Dodge, F.T. The spreading of liquid droplets on solid surfaces. J. Colloid Interface Sci. **1988**, *121*, 154–160.
21. Ondarçuhu, T.; Veyssié, M. Relaxation modes of the contact line of a liquid spreading on a surface. Nature **1991**, *352*, 418–419.
22. Dussan, E.B.; Davis, S.H. On the motion of a fluid-fluid interface along a solid surface. J. Fluid Mech. **1974**, *65*, 71–95.
23. Davis, S.H. Contact-line problems in fluid mechanics. J. Appl. Mech. **1983**, *50*, 977–982.
24. Bonn, D.L.; Eggers, J.; Indekeu, J.; Meunier, J.; Rolley, E. Wetting and spreading. Rev. Mod. Phys. **2009**, *81*, 739–805.
25. Cox, R.G. The dynamics of the spreading of liquids on a solid surface. part 1. viscous flow. J. Fluid Mech. **1986**, *168*, 169–194.
26. Teletzke, G.; Davis, H.; Scriven, L.E. Wetting hydrodynamics. Revue Phys. Appl. **1988**, *23*, 989–1007.
27. E.B. Dussan, V. The moving contact line: The slip boundary condition. J. Fluid Mech. **1976**, *77*, 665–684.
28. Huh, C.; Mason, S.G. The steady movement of a liquid meniscus in a capillary tube. J. Fluid Mech. **1977**, *81*, 401–419.
29. Mason, S. Effects of surface roughness on wetting (theoretical). J. Colloid Interface Sci. **1977**, *60*, 11–38.
30. Hardy, W.B.; Hardy, J.K. II Note on static friction and on the lubricating properties of certain chemical substances. Philos. Mag. Ser. *6* **1919**, *38*, 32–48.
31. Benner, R.; Teletzke, G.; Scriven, L. Reply to "A comment on the order of the wetting transition at a solid–fluid interface". J. Chem. Phys. **1984**, *80*, 587–589.
32. Hoang, A.; Kavehpour, H. Dynamics of nanoscale precursor film near a moving contact line of spreading drops. Phys. Rev. Lett. **2011**, *106*, 1–4.
33. Bretherton, F.P. The motion of long bubbles in tubes. J. Fluid Mech. **1961**, *10*, 166–188.
34. Hoffman, R.L. A study of the advancing interface. I. Interface shape in liquid–gas systems. J. Colloid Interface Sci. **1975**, *50*, 228–241.
35. Lelah, M.D.; Marmur, A. Spreading kinetics of drops on glass. J. Colloid Interface Sci. **1981**, *82*, 518–525.
36. Tanner, L.H. The spreading of silicone oil drops on horizontal surfaces. J. Phys. D Appl. Phys. **1979**, *12*, 1473–1484.
37. de Gennes, P.G.; Levinson, P. Dynamics of wetting: Local contact angles. J. Fluid Mech. **1990**, *212*, 55–63.
38. Voinov, O.V. The energy equation in wetting hydrodynamics. Fluid Dyn. **1996**, *31*, 891–896.
39. Kalliadasis, S.; Chang, H.-C. Dynamics of liquid spreading on solid surfaces. Ind. Eng. Chem. Res. **1996**, *35*, 2860–2874.
40. Yeo, L.Y.; Chang, H.-C. Electrowetting films on parallel line electrodes. Phys. Rev. E **2006**, *73*, 011605.
41. Veretennikov, I.; Indeikina, A.; Chang, H.-C. Front dynamics and fingering of a driven contact line. J. Fluid Mech. **1998**, *373*, 81–110.
42. Moffatt, H.K. Viscous and resistive eddies near a sharp corner. J. Fluid Mech. **1964**, *18*, 1–18.
43. Lamb, H. *Hydrodynamics*; Cambridge University Press: Cambridge, 1932.
44. Benjamin, T.B.; Ursell, F. The stability of the plane free surface of a liquid in vertical periodic motion. Proc. R. Soc. Lond. A **1954**, *225*, 505–515.
45. Xu, J.; Attinger, D. Acoustic excitation of superharmonic capillary waves on a meniscus in a planar microgeometry. Phys. Fluids **2007**, *19*, 108107.
46. Scortesse, J.; Manceau, J.F.; Bastien, F. Interaction between a liquid layer and vibrating plates: Application to the displacement of liquid droplets. J. Sound Vib. **2002**, *254*, 927–938.
47. Noblin, X.; Buguin, A.; Brochard-Wyart, F. Triplon modes of puddles. Phys. Rev. Lett. **2005**, *94*, 1–4.
48. Noblin, X.; Buguin, A.; Brochard-Wyart, F. Vibrated sessile drops: Transition between pinned and mobile contact line oscillations. Eur. Phys. J. E **2004**, *14*, 395–404.
49. Lyubimov, D.V.; Lyubimova, T.P.; Shklyaev, S.V. Behavior of a drop on an oscillating solid plate. Phys. Fluids **2006**, *18*, 012101.
50. Fayzrakhmanova, I.S.; Straube, A.V. Stick-slip dynamics of an oscillated sessile drop. Phys. Fluids **2009**, *21*, 072104.
51. Brunet, P.; Eggers, J.; Deegan, R.D. Motion of a drop driven by substrate vibrations. Euro. Phys. J.-Special Topics **2009**, *166*, 11–14.
52. Daniel, S.; Chaudhury, M.K.; de Gennes, P.G. Vibration-actuated drop motion on surfaces for batch microfluidic processes. Langmuir **2005**, *21*, 4240–4248.
53. Beyer, R.T. Parameter of nonlinearity in fluids. J. Acoust. Soc. Am. **1960**, *32*, 719–721.
54. Hamilton, M.F.; Blackstock, D.T. *Nonlinear Acoustics*; Academic Press: New York, 1998.
55. Morse, P.M.; Ingrad, K.U. *Theoretical Acoustics*; Princeton University: Princeton, NJ, 1968.
56. Biwersi, S.; Manceau, J.F.; Bastien, F. Displacement of droplets and deformation of thin liquid layers using flexural vibrations of structures. influence of acoustic radiation pressure. J. Acoust. Soc. Am. **2000**, *107*, 661–664.

57. Bennès, J.; Alzuaga, S.; Chabé, P.; Morain, G.; Chérioux, F.; Manceau, J.F.; Bastien, F. Action of low frequency vibration on liquid droplets and particles. Ultrasonics **2006**, *44*, e497–e502.
58. Brunet, P.; Eggers, J.; Deegan, R. Vibration-induced climbing of drops. Phys. Rev. Lett. **2007**, *99*, 144501.
59. Chu, B.T.; Apfel, R.E. Acoustic radiation pressure produced by a beam of sound. J. Acoust. Soc. Am. **1982**, *72*, 1673–1687.
60. King, L.V. On the acoustic radiation pressure on spheres. Proc. R. Soc. Lond. A **1934**, *147*, 212–240.
61. Eckart, C. Vortices and streams caused by sound waves. Phys. Rev. **1948**, *73*, 68–76.
62. Nyborg, W.L. Acoustic streaming due to attenuated plane waves. J. Acous. Soc. Am. **1952**, *25*, 1–8.
63. Manor, O.; Dentry, M.; Friend, J.R.; Yeo, L.Y. Substrate dependent drop deformation and wetting under high frequency vibration. Soft Matter **2011**, *7*, 7976–7979.
64. Kang, K.H. How electrostatic fields change contact angle in electrowetting. Langmuir **2002**, *18*, 10318–10322.
65. Kim, P.; Duprat, C.; Tsai, S.S.H.; Stone, H.A. Selective spreading and jetting of electrically driven dielectric films. Phys. Rev. Lett. **2011**, *107*, 034502.
66. Yeo, L.Y.; Chang, H.-C. Static and spontaneous electrowetting. Modern Phys. Lett. B **2005**, *19*, 549–569.
67. Rezk, A.R.; Manor, O.; Friend, J.R.; Yeo, L.Y. Unique fingering instabilities and soliton-like wave propagation in thin acoustowetting films. Nature Commun. **2012**, *3*, 1167.
68. Collins, D.J.; Manor, O.; Winkler, A.; Schmidt, H.; Friend, J.R.; Yeo, L.Y. Atomization off thin water films generated by high frequency substrate wave vibrations. Phys. Rev. E **2012**, *86*, 056312.